Journal of Petroleum Exploration and Production Technology (2018) 8:1069–1078
https://doi.org/10.1007/s13202-018-0464-1

ORIGINAL PAPER - EXPLORATION ENGINEERING

Analysis and optimization of control algorithms for RSS^{TSP} for horizontal well drilling

Li Gang Zhang[1,3] · G. R. Liu[2,3] · Wei Li[1] · Shi Bin Li[1]

Received: 28 November 2017 / Accepted: 4 April 2018 / Published online: 13 April 2018

Abstract

Steering control algorithm plays an important role in a rotary steerable system for horizontal well drilling, including the determination of the well trajectory, vibrations, stability, durability among other variables. This work develops a control algorithm for three static push-the-bit rotary steerable systems (RSS^{TSP}) (TSP is the abbreviation of "three static push-the-bit"). Based on the structure, mechanism, and working process of the RSS^{TSP}, mechanical and mathematical models are proposed to determine the required steering force (amplitude and direction) to move the drill bit from a point to another. Additional equations are constructed to overcome the non-uniqueness and then compute the optimal forces for the three pads to achieve the required steering force. Moreover, a new control algorithm of RSS^{TSP} is developed, considering the steerability, stability, durability, favorable area, unfavorable area, maximum usable magnitude of steering force. The proposed control algorithm is also applied to a new RSS^{TSP} and tested on a GU-693-P102 well for validation. It is found that each pad force changes smoothly, the drilling tool is stable, and the well trajectory is consistent with the design, demonstrating that our proposed control algorithm is robust and effective for RSS^{TSP} for horizontal well drilling.

Keywords Horizontal well drilling · Rotary steerable system (RSS^{TSP}) · Control algorithm · Steering force · Pad force · Dogleg

Introduction

With the technological development for unconventional oil and natural gas productions, the numbers of horizontal and three-dimensional multi-target directional wells have increased significantly (Ozkan et al. 2011; Jia et al. 2014; Orem et al. 2014). Drilling equipment not only needs to meet requirements for desired drilling trajectory, but also needs to work reliably in more complex stratum and harsher operating conditions, which presents significant challenges on the drilling technology (John et al. 2000; Kaiser and Yu 2015; Ikonnikova et al. 2015). In recent decades, rotary steerable systems (RSS) have developed very rapidly, in their capability to provide continuous rotation, constant steering, and smoother boreholes (Weijermans et al. 2001; Drummond et al. 2007; Hakam et al. 2014). RSS ensure steering the borehole when drill string is rotating, and are usually used together with a logging while drilling (LWD) system. Geological parameters are analyzed in real time, and then precise control of the directional trajectory is achieved based on geological conditions (Haugen 1998; Tribe et al. 2001; Torsvoll et al. 2010). So far, Schlumberger's PowerDrive, Baker Hughes' AutoTrak, and Halliburton's Geo-Pilot have been the main representative technologies (Stuart et al. 2000; Tribe et al. 2001; Bian et al. 2011; Wang et al. 2014). RSS can be divided into static bias and dynamic bias according to different bias units and can also be divided into push-the-bit and point-the-bit approaches according to different directing principles. PowerDrive and AutoTrak belong to "push-the-bit," while Geo-Pilot belongs to "point-the-bit" type. PowerDrive is of dynamic bias, while AutoTrak is of static bias (Schaaf 2000; Fontenot et al. 2005; Wang et al. 2014). This article focuses on three static push-the-bit (RSS^{TSP}) like AutoTrak systems. RSS^{TSP} have three stretching pads, which press against the well bore thereby causing the bit to press on the opposite side resulting in a direction change (Niu et al.

✉ Li Gang Zhang
zhangligang529@163.com

[1] Department of Petroleum Engineering, Northeast Petroleum University, Daqing, China

[2] School of Mechanical Engineering, Hebei University of Technology, Tianjin, China

[3] Department of Aerospace Engineering and Engineering Mechanics, University of Cincinnati, Ohio, USA

2013; Wang et al. 2014, Marck and Detournay 2016). Steering control algorithm plays an important role in any RSS^{TSP}, and a robust control algorithm is the key factor to achieve the desired control effects (Seifabad and Ehteshami 2013; Hakam et al. 2014; Kremers et al. 2015).Because many of these techniques are not available to the public, the research papers for control algorithm for RSS^{TSP} are very few in the published literature. Zhang and Yu analyzed the configuration and deviation principle of RSS^{STP} (Zhang 2000). Cheng and Jiang studied control method, using biasing displacement vector (Cheng et al. 2010). Du and Liu studied multi-solution and uncertainty for controlling three pad forces. Models were established with two pads and adapted to adjust and control magnitude and orientation of steering force vector, and another pad extended to wellbore without force (Du et al. 2008). Due to non-unique solutions, Li et al. (2015) proposed to use three pads working at the same time, where one pad force should have a maximum or minimum value determined by relative position of pad and steering forces. The aforementioned papers mainly deal with how to calculate steering force. However, vibrations, stability, and durability were not considered. Therefore, based on the structure and work process of RSS^{TSP}, this work develops mechanical and mathematical models for the steering force and pad force. A new control algorithm is developed considering factors of steerability, stability, durability, "favorable area," and "unfavorable area."

Structure and work process of RSS^{TSP}

RSS^{TSP} has three support pads: pad 1, 2, and 3, which are spaced 120° apart from each other, as shown in Fig. 1a, with coordinated movements for rotating spindle, drill string, and bit rotating. The pads are relative static to the rotating outside sleeve. The pads are driven by drilling fluid and stretched out to press against the well bore, thereby causing the bit to press on the opposite side causing a direction change. The support force for each pad is expressed as F_1, F_2, F_3, respectively, as shown in Fig. 1b. The resultant force F of three pad forces forms the total steering force, leading to desired changes in inclination and azimuth, as shown in Fig. 1c.

The RSS^{TSP} works as follows: The value and direction of steering force are first determined based on the current actual point and the expected point on the ground. The steering force is then transmitted downhole. Based on steering force, each pad force is next determined in accordance with predetermined control algorithms downhole. Lastly, the pads are pushed out by applying hydraulic pressure, and the expected steering force and well trajectory are realized. In the whole process, a robust algorithm for steering force and pad force is the key factor for achieving the desired control effects.

Maximum usable steering forces (A_{max})

For a given hydraulic pressure applied, the static bias pad has a maximum or minimum support force (F_{max} or F_{min}). Because the three pads are 120° apart, the range of the steering force is in a hexagon, as shown in Fig. 2a, b. The hexagon shall have an inner circle and an outer circle, as shown in Fig. 2c.

For a given position of the three pads, if the maximum usable magnitude of steering force (A_{max}) is within the inner circle and outer circle touching the hexagon, it can only be realized at a point on the hexagon, as shown in Fig. 3. If the steering force is within the inner circle, it can be achieved everywhere. In the actual operation, in order to achieve a steering force in all directions at any time, the steering force must be adjustable in 360°. Therefore, the steering force should be limited in the range within the inner circle. Thus, the maximum usable magnitude of steering force is not F_{max}, but A_{max} shown in Fig. 3.

The maximum usable magnitude of steering force can be expressed as follows:

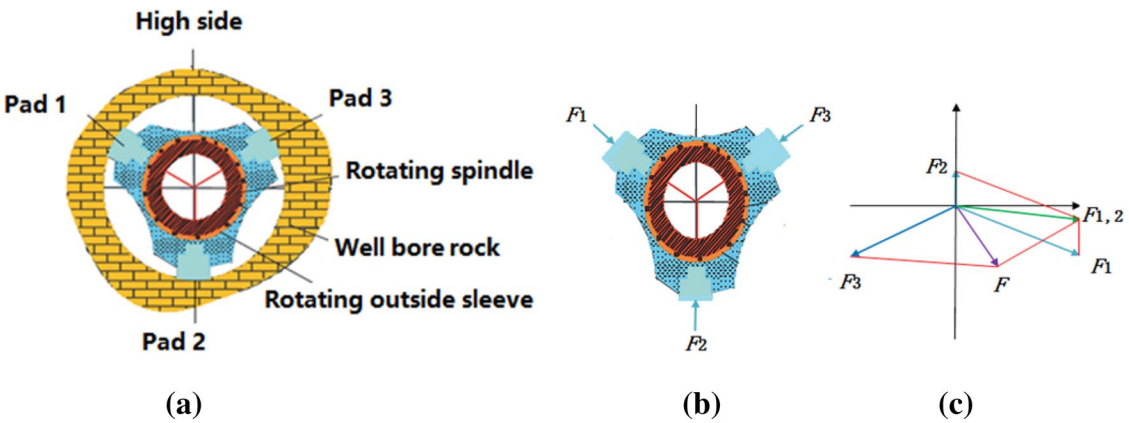

Fig. 1 Schematic of the structure and pad forces of a typical RSS^{TSP}

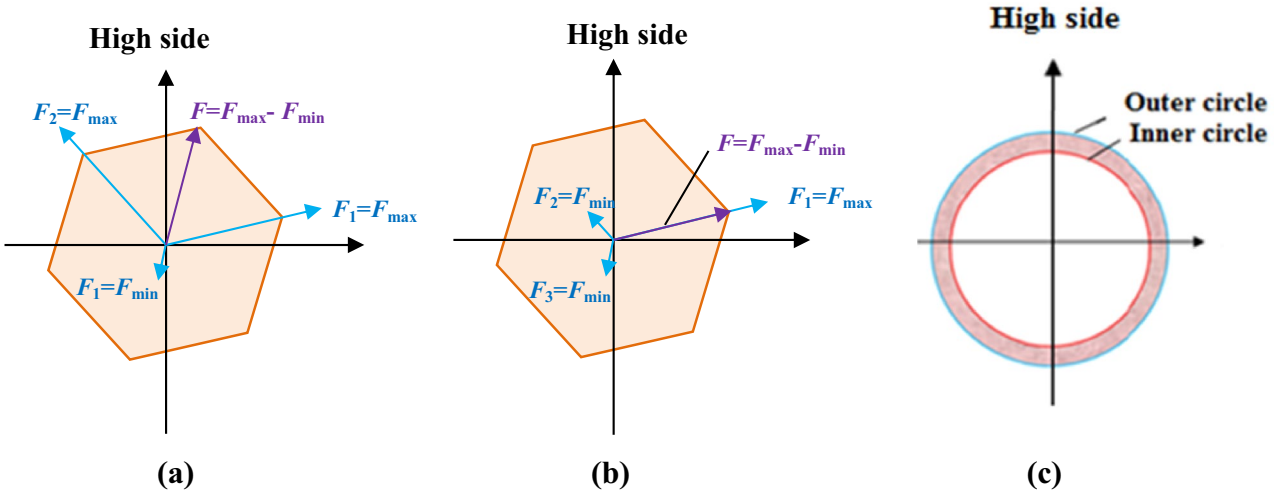

Fig. 2 Inner circle and outer circle hosting the hexagon of maximum pad force

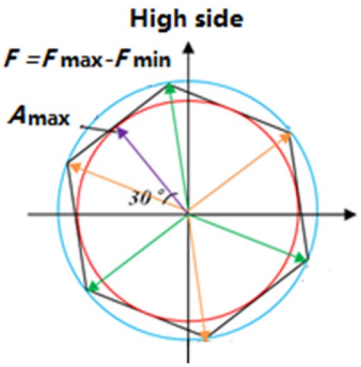

Fig. 3 Vector geometry of the maximum steering force

$$A_{\max} = \frac{\sqrt{3}}{2} \times (F_{\max} - F_{\min}), \tag{1}$$

where F_{max} is the maximum support force of the pad, F_{min} is the minimum support force of the pad, and A_{max} is the maximum usable magnitude of steering force. It is necessary to consider the constraint of A_{max} in the control algorithm, so as to achieve a desired dogleg, build rate, or walk rate in the actual operations.

Amplitude and direction of the required steering force

Consider a RSS[TSP] used in a drilling operation. The amplitude and its direction of the required steering force should be determined based on the current point and orientation of the drill bit and the target point and orientation one would want the drill bit to be.

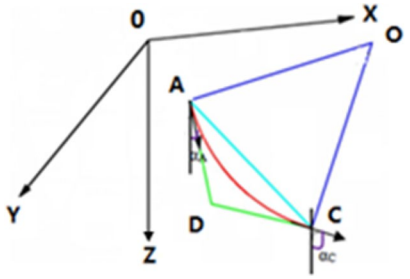

Fig. 4 Current position "A" and targeted position "C"

Amplitude of the required steering force (A_k)

Assume that the current drill bit is at point A (X_A, Y_A, Z_A), and the actual hole inclination angle and azimuth angle are α_A and β_A. The targeted position is at point C (X_C, Y_C, Z_C), and the expected inclination angle and azimuth angle are α_C and β_C. The tangent lines at points A and C intersect at point D, and the normal lines of points A and C intersect at point O, as shown in Fig. 4.

Let the changes in inclination angle and azimuth angle be $\Delta\alpha_{AC}$ and $\Delta\beta_{AC}$, and the average inclination angle of points A and C be α_0. The γ of points A and C can be calculated as follows:

$$\gamma = \frac{30 \times 360 \left| \sin \frac{\sqrt{\Delta\alpha_{AC}^2 + \Delta\beta_{AC}^2 \cdot \sin\alpha_0^2}}{2} \right|}{\pi\sqrt{(X_C - X_A)^2 + (Y_c - Y_A)^2 + (Z_C - Z_A)^2}}, \tag{2}$$

where $\Delta\alpha_{AC} = \alpha_C - \alpha_A$, $\Delta\beta_{AC} = \beta_C - \beta_A$, $\alpha_0 = \frac{\alpha_A + \alpha_C}{2}$, γ is the dogleg, α_A is the inclination angle of point "A," α_c is the

inclination angle of point "C," and α_o is the average inclination angle.

The γ_{max} of RSS^{TSP} is usually known and supplied by manufactures under A_{max}. The work efficiency of RSS^{TSP} is defined as follows:

$$A_k = \frac{\gamma}{\gamma_{max}} \times 100\%, \tag{3}$$

where γ_{max} is the dogleg when working under A_{max}.

If the value of A_k is greater than 100%, it would not be drilled to the target point. In this situation, it is necessary to redesign well trajectory and redetermine target point until the value of A_k is less than 100%.

It can also be expressed using the amplitudes of the steering forces in relation to its maximum usable magnitude, as follows:

$$A_k = \frac{F}{A_{max}} \times 100\%, \tag{4}$$

where F is the steering force.

Therefore, once A_k is obtained, the amplitude of the steering force F can be calculated using Eq. (4).

Direction of steering force (α_k)

The direction angle of steering force (α_k) is defined as clockwise rotation angle from high side to the direction of steering force in the bottomhole plane. The steering force could be broken up into build force and walk force, as shown Fig. 5.

The "+" indicates increase in "build force" or "walk force," and the "−" indicates decrease in "build force" or "walk force." Build rate and walk rate are also determined by steering force and the direction angle of steering force α_k.

With the current point (A) and expected point (C) shown in Fig. 4, the expected build rate ($\Delta\alpha$) and the walk rate ($\Delta\beta$) can be obtained using

$$\Delta\alpha = 30 \times \frac{\alpha_c - \alpha_A}{\Delta D_m}, \tag{5}$$

$$\Delta\beta = 30 \times \frac{\beta_c - \beta_A}{\Delta D_m}, \tag{6}$$

where $\Delta\alpha$ is the expected build rate, β_A is the azimuthal angle of point "A," β_c is the azimuthal angle of point "A," β_o is the average azimuthal angle, and $\Delta\beta$ is the expected walk rate.

The relations between dogleg γ and α_K, $\Delta\alpha$ and $\Delta\beta$ (Lapeyrouse et al. 2002) are shown in Fig. 6.

Figure 6 shows graphic relationship between α_K $\Delta\beta$, α_0, and $\Delta\alpha$. According to the changes in the inclination and azimuth, α_K can be divided into following nine cases:

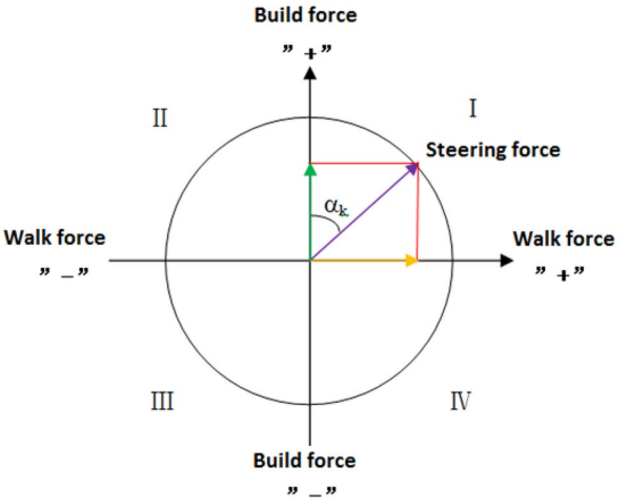

Fig. 5 steering force distribution in bottomhole plane

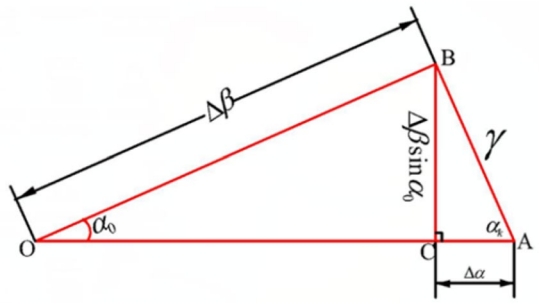

Fig. 6 Diagram for calculating dogleg

$$_{k} = \begin{pmatrix} 0, (\Delta\alpha > 0, \Delta\beta = 0), (1) \\ \arctan\left(\frac{\Delta\beta \times \sin\alpha 0}{\Delta\alpha}\right), (\Delta\alpha > 0, \Delta\beta > 0), (2) \\ 90, (\Delta\alpha = 0, \Delta\beta > 0), (3) \\ \arctan\left(\frac{\Delta\beta \times \sin\alpha 0}{\Delta\alpha}\right) + 180, (\Delta\alpha < 0, \Delta\beta > 0), (4) \\ 180, (\Delta\alpha < 0, \Delta\beta = 0), (5) \\ \arctan\left(\frac{\Delta\beta \times \sin\alpha 0}{\Delta\alpha}\right) + 180, (\Delta\alpha < 0, \Delta\beta < 0), (6) \\ 270, (\Delta\alpha = 0, \Delta\beta < 0), (7) \\ \arctan\left(\frac{\Delta\beta \times \sin\alpha 0}{\Delta\alpha}\right) + 360, (\Delta\alpha < 0, \Delta\beta < 0), (8) \\ None, (9) \end{pmatrix} \tag{7}$$

1. Full working to advance the inclination, while the azimuth is not changed.
2. Both the inclination angle and azimuth angle are all advanced.

3. Full working to increase azimuth, while the inclination is not changed.
4. The inclination angle decreased, while the azimuth angle increased.
5. Full working to decrease inclination angle, while the azimuth angle is not changed.
6. The inclination angle and the azimuth angle all decreased.
7. Full working to decrease azimuth, while the inclination is not changed.
8. The inclination angle and the azimuth angle all decreased.
9. No working. The inclination and the azimuth were controlled by BHA.

A new algorithm for pad forces (F_1, F_2, F_3)

Non-uniqueness for pad forces

When the amplitude A_k and the direction α_k of the required steering force F are determined, a control algorithm is then needed to adjust each pad force to achieve the required steering force. The control variables are these three pad forces. These force vectors constitute a planar concurrent force system in the bottomhole plane, as shown in Fig. 7.

Figure 7 shows two programs which adjust three pad forces (F_1, F_2, F_3) or (F_1', F_2', F_3') to achieve the same required steering force F. F_{12} is the resultant force of F_1 and F_2. F_{12}' is the resultant force of F_1' and F_2'. The relation between F and F_1, F_2, F_3 can be expressed as follows:

$$\begin{cases} F\cos\alpha_k = F_1\cos\alpha_1 + F_2\cos(\alpha_1+240) + F_3\cos(\alpha_1+120) \\ F\sin\alpha_k = F_1\sin\alpha_1 + F_2\sin(\alpha_1+240) + F_3\sin(\alpha_1+120) \end{cases} \tag{8}$$

The angle (α_1) between pad 1 and high side is measured by the RSS^{TSP} system. Once F and α_k are determined, there are three unknown parameters F_1, F_2, and F_3. However, there are only two equations in Eq. (8). The solutions are thus not unique. To determine F_1, F_2, and F_3, an additional equation must be established.

An additional equation for optimal pad force

When a RSS^{TSP} starts to work, in order to prevent pad damages, forces exerted on each pad should be limited. Initially, the three pads should start simultaneously with the same forces. The initial force can be set as,

$$F_{ini} = \frac{F_{max} + F_{min}}{2}, \tag{9}$$

where F_{ini} is the pad force at the initial working time.

When the RSS^{TSP} starts to steer the drill bit to a target point, we require a steering force F and direction α_K. One has to decide on whether each of the pad forces is in a "favorable" or "unfavorable" area. Such a decision is made by assessing the direction of each of the pad forces F_1, F_2, and F_3, in relation to the required steering force. If the angle between a pad force and the required steering force is within (− 30°, 30°), the pad force plays a positive role in achieving the required steering force, as shown in the hexagon in Fig. 8. In such cases, the pad force falls in the "favorable" area, and the force of the pad should be:

$$F_f = \frac{F_{max} + F_{min}}{2} + \frac{F_{max} - F_{min}}{2}A_K, \tag{10a}$$

where F_f is the pad force on the favorable area and the second term on the right-hand side of Eq. (10a) is the augment of the pad force. On the other hand, if the angle between the pad force and the opposite direction of steering force is

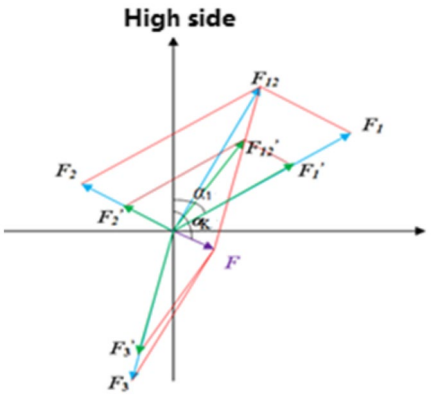

Fig. 7 Three pad forces adjusted to achieve the required steering force F

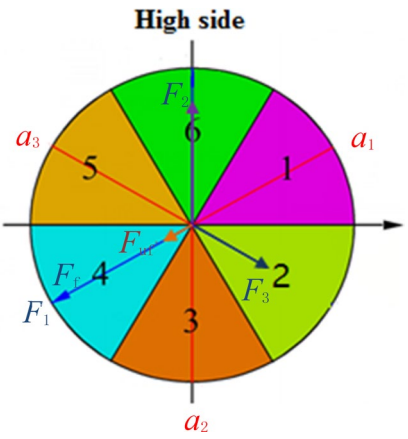

Fig. 8 Six areas of favorability based on the angle between the directions of each pad force and the required steering force

within (−30°, 30°), the pad force plays a negative role in achieving the required steering force. In such cases, the pad force falls in the unfavorable area. The pad force takes big value in favorable area and takes small value in the "unfavorable" area, and the force of the pad should be:

$$F_{\mathrm{uf}} = \frac{F_{\max} + F_{\min}}{2} - \frac{F_{\max} - F_{\min}}{2} A_K, \tag{10b}$$

where the second term on the right-hand side of Eq. (10b) is the reduction of the pad force. The F_{uf} is the pad force on the unfavorable area. The bottomhole plane can now be divided into six areas, as shown in Fig. 8. At any point in time, the steering force (determined in "Maximum usable steering forces ($A_{\max}$)" section) should fall in one of these six areas. The favorable or unfavorable area for one of the pad forces can then be easily determined.

For example, if the required steering force falls in area 1 (in which there is no pad), then area 4 (in which there must be a pad) is an unfavorable area. We thus set the pad force in area 4 with an unfavorable force: $F_1 = F_{\mathrm{uf}}$, which gives an additional equation to Eq. (8), so that a set of solutions for all the pad forces can be uniquely found. If the steering force falls in area 2 (in which there is a pad), then area 2 is the favorable area. In this case, a favorable force should be assigned to pad 2: $F_2 = F_{\mathrm{f}}$, which gives an additional equation. If the steering force is in area 3, then area 6 is the unfavorable area and $F_3 = F_{\mathrm{uf}}$ becomes an additional equation. If the steering force is in area 4, then area 4 is the favorable area and $F_1 = F_{\mathrm{f}}$ gives as an additional equation. If the steering force is in area 5, then area 2 is the unfavorable area and $F_3 = F_{\mathrm{uf}}$ becomes an additional equation. If the steering force is in area 6, then area 6 is the favorable area and $F_2 = F_{\mathrm{f}}$ becomes an additional equation.

A new algorithm for pad forces

We are now ready to develop a new algorithm for computing the pad forces. For convenience, we define a $\alpha_K' = \alpha_K - \alpha_1$, which is the relative direction of α_K with respect to α_1, as shown in Fig. 9.

As a general convention, α_1 and α_k are all defined as clockwise positive. The relative steering force direction α_K' is also defined as clockwise positive with respect to pad 1, and it can be expressed in the following two cases.

$$\begin{cases} \alpha_K' = \alpha_K - \alpha_1; & \alpha_{\mathrm{K}} \geq \alpha_1 \\ \alpha_K' = \alpha_K - \alpha_1 + 360; & \alpha_K < \alpha_1 \end{cases} \tag{11}$$

According to the relative status of the steering force, one of the pads can be determined in either the favorable and unfavorable areas, following the procedure detailed in "Direction of steering force (α_k)" section. Hence, there are six possible situations.

Situation 1: The steering force is in area 1, as shown in Fig. 10.

In Fig. 10, $F_{1\mathrm{F}}$, $F_{2\mathrm{F}}$, and $F_{3\mathrm{F}}$ are the force components in the directions of F, respectively, for F_1, F_2, and F_3. $F_{1\mathrm{f}}$, $F_{2\mathrm{f}}$, and $F_{3\mathrm{f}}$ are the force components in the normal direction of F, respectively, for F_1, F_2, and F_3. At this situation, $\alpha_K' > 330^{\circ}$ or $\alpha_K' \leq 30^{\circ}$, and pad 1 is in a unfavorable area. Then, supplying $F_1 = F_{\mathrm{uf}}$ into Eq. (8), we obtain:

$$\begin{cases} F_1 \cos(\alpha_K' - 180) + F_2 \cos(\alpha_K' - 300) + F_3 \cos(\alpha_K' - 60) = A_{\max} A_K \\ F_1 \sin(\alpha_K' - 180) + F_2 \sin(\alpha_K' - 300) + F_3 \sin(\alpha_K' - 60) = 0 \\ F_1 = F_{\mathrm{uf}} \end{cases} \tag{12}$$

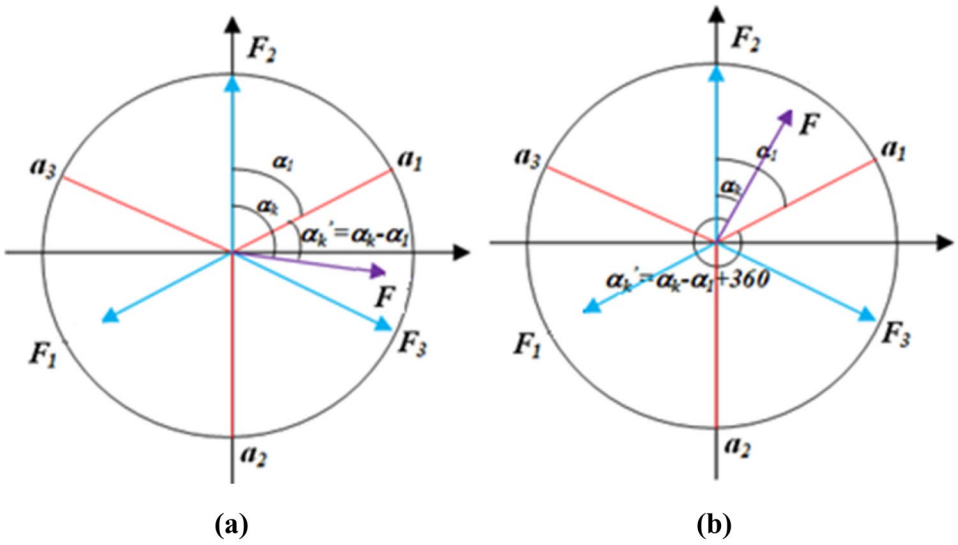

Fig. 9 Relative direction (α_k') with respect to direction α_1

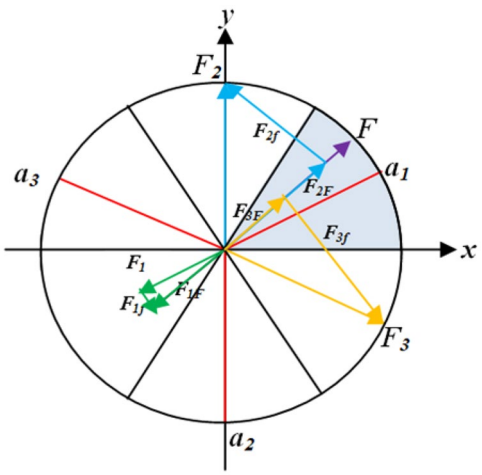

Fig. 10 Steering and pad forces when $\alpha_K^{'} > 330$ or $\alpha_K^{'} \leq 30$

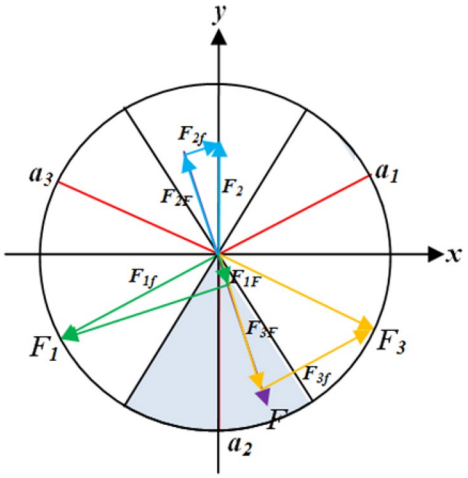

Fig. 12 Steering and pad forces when $90 < \alpha_K^{'} \leq 150$

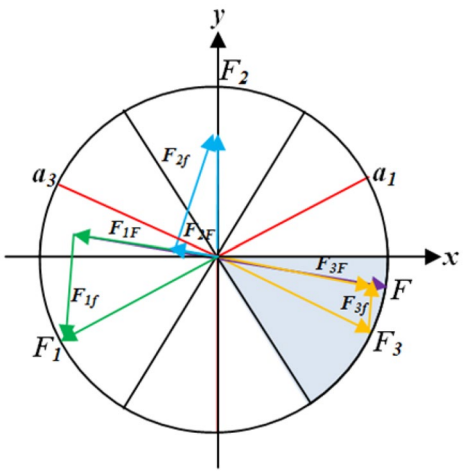

Fig. 11 Steering and pad forces when $30 < \alpha_K^{'} \leq 90$

Equation (12) now has unique solutions, and the result is as follows:

$$\begin{cases} F_1 = F_{\text{uf}} \\ F_2 = F_{\text{uf}} - \frac{2\sqrt{3}}{3} A_{\max} \sin(\alpha_k^{'} - 60) A_K \\ F_3 = F_{\text{uf}} + \frac{2\sqrt{3}}{3} A_{\max} \sin(\alpha_k^{'} + 60) A_K \end{cases} \tag{13}$$

Situation 2: The steering force is in area 2, as shown in Fig. 11.

In this situation, pad 3 is in a favorable area, and $30 < \alpha_K^{'} \leq 90^{\circ}$, which gives an additional equation of $F_3 = F_{\text{f}}$. Therefore, a unique solution can be given as follows:

$$\begin{cases} F_1 = F_{\text{f}} - \frac{2\sqrt{3}}{3} A_{\max} \sin(\alpha_k^{'} + 60) A_K \\ F_2 = F_{\text{f}} - \frac{2\sqrt{3}}{3} A_{\max} \sin(\alpha_k^{'}) A_K \\ F_3 = F_{\text{f}} \end{cases} \tag{14}$$

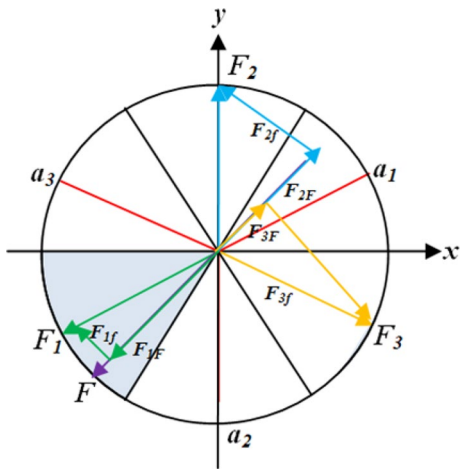

Fig. 13 Steering and pad forces when $150 < \alpha_K^{'} \leq 210$

Situation 3: The steering force is in area 3, as shown in Fig. 12.

In this situation, pad 2 is in a unfavorable area, and $90 < \alpha_{\text{K}}^{\prime} \leq 150^{o}$, which gives $F_2 = F_{\text{uf}}$. The unique solution becomes:

$$\begin{cases} F_1 = F_{\text{uf}} - \frac{2\sqrt{3}}{3} A_{\max} \sin(60 - \alpha_k^{'}) A_K \\ F_2 = F_{\text{uf}} \\ F_3 = F_{\text{uf}} + \frac{2\sqrt{3}}{3} A_{\max} \sin(\alpha_k^{'}) A_K \end{cases} \tag{15}$$

Situation 4: The steering force is in area 4, as shown in Fig. 13.

In this situation, pad 1 is in a favorable area, and $150 < \alpha_K^{'} \leq 210^{\circ}$, which supplies $F_1 = F_f$. Then, the solution is obtained as follows:

$$\begin{cases} F_1 = F_f \\ F_2 = F_f + \frac{2\sqrt{3}}{3} A_{max} \sin(60 - \alpha_k^{'}) A_K \\ F_3 = F_f + \frac{2\sqrt{3}}{3} A_{max} \sin(\alpha\alpha_k^{'} + 60) A_K \end{cases} \quad (16)$$

Situation 5: The steering force is in area 5, as shown in Fig. 14.

In this situation, pad 3 is in a favorable area, and $210 < \alpha_K^{'} \leq 270^{\circ}$, which gives an addition equation of $F_3 = F_{uf}$. Then, the result is found as follows:

$$\begin{cases} F_1 = F_{uf} - \frac{2\sqrt{3}}{3} A_{max} \sin(60 + \alpha_k^{'}) A_K \\ F_2 = F_{uf} - \frac{2\sqrt{3}}{3} A_{max} \sin(\alpha_k^{'}) A_K \\ F_3 = F_{uf} \end{cases} \quad (17)$$

Situation 6: The steering force is in area 6, as shown in Fig. 15.

In this situation, pad 2 is in a favorable area, and $270 < \alpha_K^{'} \leq 330^{o}$, which leads to an addition equation of $F_2 = F_f$. Then, the result becomes:

$$\begin{cases} F_1 = F_f - \frac{2\sqrt{3}}{3} A_{max} \sin(60 - \alpha_k^{'}) A_K \\ F_2 = F_f \\ F_3 = F_f + \frac{2\sqrt{3}}{3} A_{max} \sin(\alpha_k^{'}) A_K \end{cases} \quad (18)$$

Integrating the steer capability, stability, durability, favorable area, unfavorable area, maximum usable magnitude of steering force, a new control algorithm of RSS^{TSP} can easily be written using Eqs. (12)–(18).

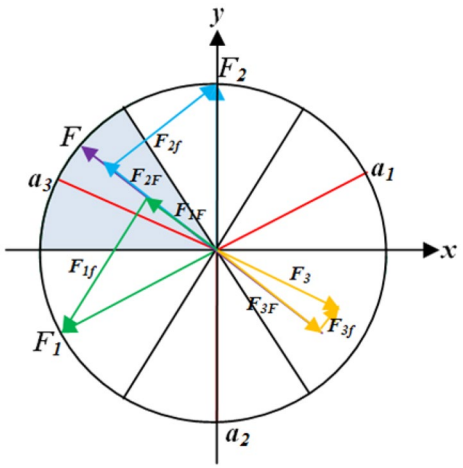

Fig. 14 Steering and pad forces when $210 < \alpha_K^{'} \leq 270$

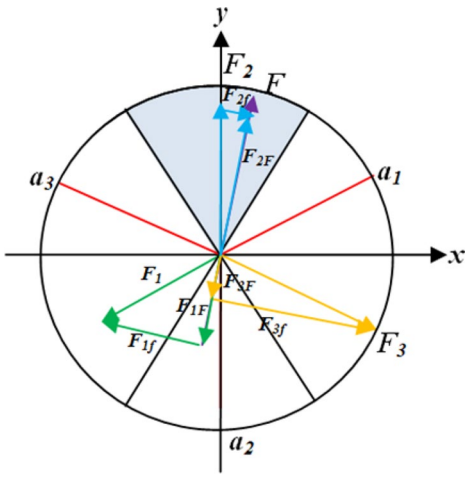

Fig. 15 Steering and pad forces when $270 < \alpha_k' \leq 330$

Field tests

The new control algorithm is applied to a RSS^{TSP} and carried out a field test in a GU-693-P102 well. The RSS^{TSP} has $F_{max} = 20$KN, and $F_{min} = 0.7$KN. If $\alpha_1 = 30$, the pad forces (F_1, F_2, F_3) are changing with the α_k based on the new control algorithm, and the outcome is plotted in Fig. 16.

It is shown that each pad force changes smoothly and decreases with decreasing A_k, which reduces drill bit vibration and improves the stability and durability of the RSS^{TSP} system. The design track and the well trajectory of GU-693-P102 are shown in Fig. 17, where the blue line is the design track and the red line is the well trajectory achieved using the present control algorithm. A is the target spot, and B is the termination spot.

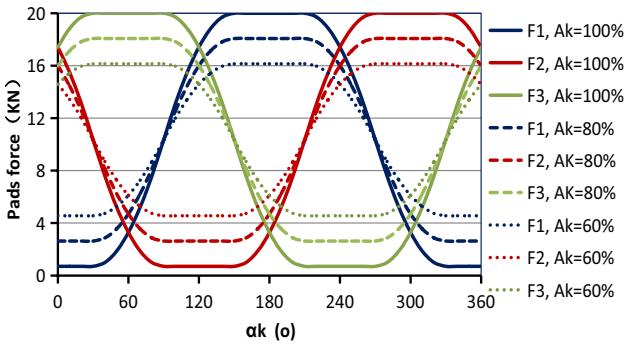

Fig. 16 Output of the pad forces controlled using the present algorithm for given different α_k

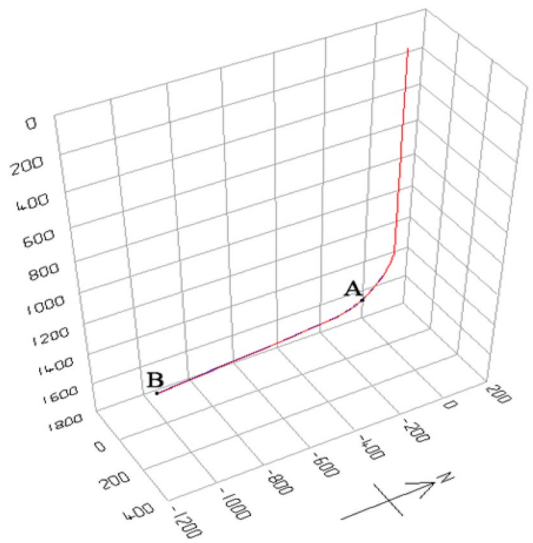

Fig. 17 Well trajectory achieved using the present algorithm against the design track

The results demonstrate the well is consistent with design track as designed. The maximum dogleg rate is 5.92°/30 m, and well trajectory is smooth. It validates that our proposed control algorithm is robust and effective for RSS^{TSP} systems.

Inclusions

1. According to the current and targeted build and walk rates, this work establishes a method to calculate the work efficiency (A_k) and direction of the required steering force (α_K). The calculated results offer key instructions to transmit from ground to downhole for a RSS^{TSP} drilling process.
2. Considering maximum usable magnitude of steering force, steerability, stability, durability, favorable area and unfavorable area, a new algorithm for assigning each pad an optimal force is developed to achieve the required steering force to move the drilling bit from point A to point B.
3. The present new control algorithm is applied to a new RSS^{TSP}, and a field test is carried out in a GU-693-P102 well for validation. It demonstrates that the new control algorithm is robust and effective for RSS^{TSP} systems.

Acknowledgements The research is mainly supported by Natural Science Foundation of Hei Long Jiang Province (No. QC2017042).

References

Bian JH, Niu WT, Wang LN et al (2011) Study of steering actuator of static "point-the-bit" rotary steerable system. In: Materials science forum, vol 697–698, pp 665–670

Cheng Z, Jiang W, Jiang S et al (2010) Control scheme for displacement vector of three-pad biasing rotary steerable system. Acta Pet Sinica 31(4):675–676

Drummond M, Costa K, Renfrow D et al (2007) Large hole RSS used for shallow kick-off, directional control in soft sediment. World Oil 228(10):39–44

Du JS, Liu B, Xia B (2008) The control scheme for three pad static bias device of push-the-bit rotary steerable system. Oil Drill Prod Technol 30(6):5–10. http://en.cnki.com.cn/Article_en/CJFDTotal-SYZC200806005.htm

Fontenot KR, Lesso B, Strickler RD et al (2005) Using casing to drill directional wells. Oilfield Rev 17(2):44–61

Hakam CE, Davis E, Serdy AM et al (2014) Rotary steerable system with optimized functionally integrated system-specific drill bits reduces drilling days and extends laterals in northeastern US Horizontal shale plays. Icarus 243:129–138

Haugen J (1998) Rotary steerable system replaces slide mode for directional drilling applications. Oil Gas J 96(9):65–71

Ikonnikova S, Gülen G, Browning J et al (2015) Profitability of shale gas drilling: a case study of the Fayetteville shale play. Energy 81:382–393

Jia C, Zhang Y, Zhao X (2014) Prospects of and challenges to natural gas industry development in China. Nat Gas Ind B 1(1):1–13

John E, Chris A, Clive D et al (2000) The application of rotary closed-loop drilling technology to meet the challenges of complex wellbore trajectories in the Janice field. SPE Drill Complet 17(3):151–158

Kaiser MJ, Yu Y (2015) Drilling and completion cost in the Louisiana Haynesville Shale, 2007–2012. Nat Resour Res 24(1):5–31

Kremers NAH, Detournay E, Wouw NVD (2015) Model-based robust control of directional drilling systems. IEEE Trans Control Syst Technol 24(1):226–239

Lapeyrouse NJ, Lyons WC, Carter T (2002) Formulas and calculations for drilling, production, and workover, 3rd edn. Elsevier, Oxford

Li SB, Wang YQ, Zhang LG, Xu YQ (2015) Analysis and optimization of static push-the-bit rotary steering control scheme. Oil Drill Prod Technol 37(4):12–15. http://www.en.cnki.com.cn/Article_en/CJFDTOTAL-SYZC201504006.htm

Marck J, Detournay E (2016) Influence of rotary-steerable-system design on borehole spiraling. SPE J 21(1):293–302

Niu WT, Li HT, Wang LN, Li YZ (2013) Static point-the-bit rotary steerable drilling tool. CN202788615 U **(Chinese)**

Orem WH, Varonka M, Crosby L et al (2014) Organic substances from unconventional oil and gas production in shale. AGU Fall Meeting Abstracts

Ozkan E, Brown ML, Raghavan R et al (2011) Comparison of fractured-horizontal-well performance in tight sand and shale reservoirs. SPE Reservoir Eval Eng 14(2):248–259

Schaaf S, Pafitis D, Guichemerre E (2000) Application of a point the bit rotary steerable system in directional drilling prototype well-bore profiles. In: SPE/AAPG western regional meeting, 19–22 June, Long Beach, California

Seifabad MC, Ehteshami P (2013) Estimating the drilling rate in Ahvaz oil field. J Pet Explor Prod Technol 3(3):1–5

Stuart S, Demos P, Eric G (2000) Application of a point the bit rotary steerable system in directional drilling prototype well-bore profiles. J Am Board Fam Med: JABFM 27(1):1400–1405

Torsvoll A, Abdollahi J, Eidem M et al (2010) Successful development and field qualification of a 9 5/8 in and 7 in rotary steerable drilling liner system that enables simultaneous directional drilling and lining of the wellbore. Phys Status Solidi 211(2):425–432

Tribe IR, Burns L, Howell PD et al (2001) Precise well placement using rotary steerable systems and LWD measurements. Am J Ophthalmol 56(5):836

Wang R, Xue Q, Han L et al (2014) Torsional vibration analysis of push-the-bit rotary steerable drilling system. Meccanica 49(7):1601–1615

Weijermans P, Ruszka J, Jamshidian H et al (2001) Drilling with rotary steerable system reduces wellbore tortuosity. Society of Petroleum Engineers, pp 194–203

Xue Q, Leung H, Wang R et al (2016) Continuous real-time measurement of drilling trajectory with new state-space models of Kalman filter. IEEE Trans Instrum Meas 65(1):144–154

Zhang SH (2000) Drilling extended reach well with rotary steering drilling system. Acta Pet Sinica 21(1):76–80